

Absence of Luther-Emery Superconducting Phase in the Three-Band Model for Cuprate Ladders

Jeong-Pil Song and Sumit Mazumdar

Department of Physics, The University of Arizona Tucson, AZ 85721

R. Torsten Clay

*Department of Physics & Astronomy, and HPC² Center for Computational Sciences,
Mississippi State University, Mississippi State, MS 39762*

(Dated: today)

Correlated-electron theories of superconductivity in layered cuprates often start from the premise of a gapped spin-liquid phase proximate to the superconducting state. This assumption is justified based on analytical and numerical demonstrations of a superconducting Luther-Emery phase in the doped 2-leg one-band Hubbard ladder, and the perceived analogy between coupled ladders and the two dimensional CuO_2 layer. We demonstrate from accurate density matrix renormalization group studies the absence of the superconducting Luther-Emery phase in the doped 2-leg three-band ladder consisting of both copper and oxygen, even as the spin gap is large in the undoped three-band ladder. For realistic oxygen-oxygen hopping and Hubbard repulsion on the oxygen atoms, density-density rather than pairing correlations are dominant at long range. This result is equally valid whether or not the oxygens outside the ladder proper, over and above the rung and leg oxygens, are included in the computation. These results demonstrate the critical importance of oxygen orbitals, and raise disturbing questions about the applicability of many of the existing correlated-electron theories of superconductivity.

I. INTRODUCTION

More than three decades after the discovery of high temperature superconductivity (SC) in cuprates, there is no consensus on the mechanism of the phenomenon. There is broad agreement that the undoped parent antiferromagnetic compounds can be described within the Cu-only one-band two-dimensional (2D) Hubbard model, which ignores the O-ions entirely. Proximity of SC to antiferromagnetism has led to the widely held belief that the mechanism of SC can also be found within an effective weakly-doped single-band Hubbard model [1–4] based on the claim that the spins on the Cu-sites and on the dopant-induced holes on the O-sites form local spin-singlets that behave like double occupancies in the single-band Hubbard model [5]. The list of approximate correlated-electron theories that find SC within the weakly doped one-band Hubbard model is long, but accurate numerical studies have consistently found that superconducting correlations are suppressed by the Hubbard U for carrier concentrations believed to be appropriate for the superconductors [6, 7]. Recent very careful study using two distinct and complementary numerical approaches to calculating superconducting pair-pair correlations has concluded that SC is absent in the square lattice Hubbard model proximate to $\frac{1}{2}$ -filling [8]. Inclusion of second neighbor hopping t' beyond nearest neighbor (n.n.) does not change this conclusion [9, 10]. Signatures of pair-correlations enhanced by the Hubbard U have been found uniquely at $\frac{1}{4}$ -filling [11], far from the carrier concentration believed to be appropriate for the cuprates. A recent density matrix renormalization group (DMRG) calculation has claimed transition from p -wave to d -wave SC within the hole-doped triangular lattice

Hubbard model, but once again at fillings very far away from $\frac{1}{2}$ [12].

A key reason for the continued application of the one-band Hubbard model to cuprates is the repeated finding that the ground state of the weakly doped 2-leg one-band Hubbard ladder is a Luther-Emery liquid, with gapless charge and gapped spin modes [13–19]. Such a spin-gap proximity effect has been considered essential for SC within an entire class of theories [1, 3, 17, 20]. DMRG calculations, highly precise for one dimensional (1D) Hamiltonians, find slower than $1/r$ decay of the superconducting pair-pair correlation $P(r)$ in the doped 2-leg one-band Hubbard ladder, where r is the interpair separation [14, 15, 18, 19]. Power law decay slower than $1/r$ is a requirement as well as signature of quasi-long range order in one dimension [21]. Strong superconducting correlations in the doped ladder is a consequence of spin-singlet formation on the undoped ladder rungs [22]. The DMRG results therefore have lent credence to the viewpoint that some variant of the 2D one-band Hubbard model with minor modifications might still yield

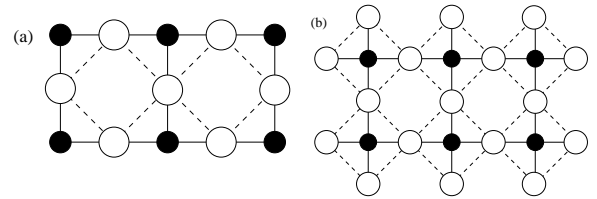


FIG. 1. Cuprate ladder geometries considered by us. Filled (open) circles represent copper (oxygen) atoms. (a) Ladder with three oxygen atoms per rung. (b) Ladder with five oxygen atoms per rung.

SC.

A realistic description of the cuprate ladder, however, should include the oxygen(O)-ions (see Fig. 1). Surprisingly, few authors have investigated the appropriateness of replacing the more complete three-band 2-leg ladder Hamiltonian that includes the O-ions with the one-band Hubbard Hamiltonian [23, 24]. We have performed accurate DMRG calculations on long three-band 2-leg ladders for parameters appropriate for real cuprates. In order to reach the longest ladders possible, we have performed the bulk of our calculations for the geometry of Fig. 1(a), with three O-ions per ladder rung. We have also performed limited calculations of superconducting pair correlations for a shorter ladder with the geometry of Fig. 1(b), with O-ions outside the ladder bonded to the Cu sites [24]. We find that the distance-dependence of the superconducting pair correlations are independent of geometry, and are strongly suppressed for both geometries of Fig. 1 at the doping traditionally assumed to correspond to the maximum of the superconducting dome within a one-band picture, $\delta \sim 0.125$. We further determine the Luther-Emery correlation exponent, κ_ρ , in the thermodynamic limit through fits of the charge density, finding $\kappa_\rho < 1$ for $\delta = 0.125$, consistent with the suppression of pairing. We present physical arguments within an effective Hamiltonian that explain the suppression of the superconducting pair correlations and their rapid decay. These results have profound implications for any realistic modeling of cuprates.

II. THEORETICAL MODEL, PARAMETERS AND COMPUTATIONAL TECHNIQUES

The one-band ladder Hamiltonian has parameters U , the Hubbard repulsion; and the leg and rung hopping integrals t and t_\perp , respectively. It is customary to express U and $|t_\perp|$ in units of $|t|$. Here we consider the three-band

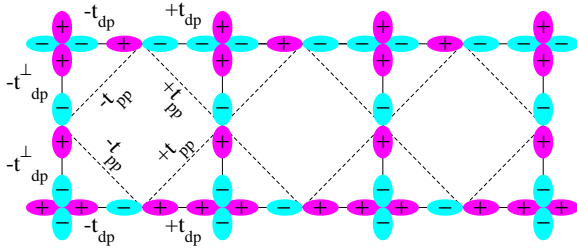


FIG. 2. (Color online) Orbital parity and sign convention for the hopping matrix elements for the ladder geometry of Fig. 1(a). Orbital parity and signs for the lattice of Fig. 1(b) follow a similar convention (see text).

ladder Hamiltonian,

$$\begin{aligned}
 H = & \Delta_{\text{dp}} \sum_{i\sigma} p_{i,\sigma}^\dagger p_{i,\sigma} + \sum_{\langle ij \rangle, \lambda, \sigma} t_{\text{dp}}^{\perp, i, j} (d_{i, \lambda, \sigma}^\dagger p_{j, \sigma} + H.c.) \\
 & + \sum_{\langle ij \rangle, \lambda, \sigma} t_{\text{dp}}^{i, j} (d_{i, \lambda, \sigma}^\dagger p_{j, \sigma} + H.c.) + \sum_{\langle ij \rangle, \sigma} t_{\text{pp}}^{i, j} (p_{i, \sigma}^\dagger p_{j, \sigma} + H.c.) \\
 & + U_{\text{d}} \sum_{i, \lambda} d_{i, \lambda, \uparrow}^\dagger d_{i, \lambda, \uparrow} d_{i, \lambda, \downarrow}^\dagger d_{i, \lambda, \downarrow} + U_{\text{p}} \sum_j p_{j, \uparrow}^\dagger p_{j, \uparrow} p_{j, \downarrow}^\dagger p_{j, \downarrow}
 \end{aligned} \tag{1}$$

Here $d_{i, \lambda, \sigma}^\dagger$ creates a hole with spin σ on the i th Cu $d_{x^2-y^2}$ orbital on the λ -th leg ($\lambda = 1, 2$), $p_{j, \sigma}^\dagger$ creates a hole on the n.n. rung oxygen O_{R} or leg oxygen O_{L} ; $t_{\text{dp}}^{\perp, i, j}$ and $t_{\text{dp}}^{i, j}$ are n.n. ladder rung and leg Cu-O hopping integrals and $t_{\text{pp}}^{i, j}$ is the n.n. O-O hopping integral. For the lattice of Fig. 1(a), the Cu-O hopping matrix elements along the legs of the ladder have the sign convention $t_{\text{dp}}^{i, j} = -t_{\text{dp}}$ for $j = i + \hat{x}/2$ and $= t_{\text{dp}}$ for $j = i - \hat{x}/2$. Along the rungs of the ladder $t_{\text{dp}}^{\perp, i, j} = -t_{\text{dp}}^\perp$. Similarly $t_{\text{pp}}^{i, j} = \pm t_{\text{pp}}$, with the plus and minus signs occurring for $j = i + \hat{x}/2 \pm \hat{y}/2$ and $j = i - \hat{x}/2 \pm \hat{y}/2$, respectively (see Fig. 2). For the lattice of Fig. 1(b) we choose the orbital parities so that the added $t_{\text{dp}}^{\perp, i, j}$ bonds are $-t_{\text{dp}}^\perp$ and the added $t_{\text{pp}}^{i, j}$ are positive and negative for $j = i - \hat{x}/2 \pm \hat{y}/2$ and $j = i + \hat{x}/2 \pm \hat{y}/2$, respectively.

U_{d} and U_{p} are the onsite repulsions on the Cu and O sites, and $\Delta_{\text{dp}} = \epsilon_p - \epsilon_d$ where ϵ_p (ϵ_d) is the site energy of O (Cu). In what follows all energies are in units of $|t_{\text{dp}}|$. Most of our calculations are for $t_{\text{dp}} = t_{\text{dp}}^\perp = 1$, $U_{\text{d}} = 8$, $\Delta_{\text{dp}} = 3$; we show a few results also for $t_{\text{dp}}^\perp > 1$. We show results for $t_{\text{pp}} = 0$ and 0.5, for two different $U_{\text{p}} = 0, 3$; the parameter set $t_{\text{pp}} = 0.5, U_{\text{p}} = 3$ is nearly identical to those used previously [23, 24]. We also show results of calculations of superconducting pair correlations for the parameters $t_{\text{pp}} = 0.6, U_{\text{p}} = 4$, as these are very close to those derived from recent first principles calculations [25]. Our calculations are performed for different dopings δ , where $1 + \delta$ is the average hole concentration per Cu-ion ($\delta = 0$ for the undoped ladder).

Our DMRG calculations are done with open boundary conditions, with Cu-O-Cu rungs at both ends (see Fig. 1(a)). Calculations used the ITensor library [26] with a two-site DMRG update, particle number and S_z conservation, and real-space parallelization [27]. For the geometry of Fig. 1(a), we have considered ladders with length L up to $L=40$ (198 sites) for the undoped case, and with up to $L = 96$ (478 sites) for doped cases, with bond dimension m up to 19,000. The minimum DMRG truncation error was of order 10^{-8} ; we extrapolated energies and correlation functions to zero truncation error as detailed in [28]. For the geometry of Fig. 1(b), our calculations of superconducting pair correlations (see below) are for $L = 64$ (450 sites). These calculations are for the longest ladders containing both Cu and O with the largest m to date.

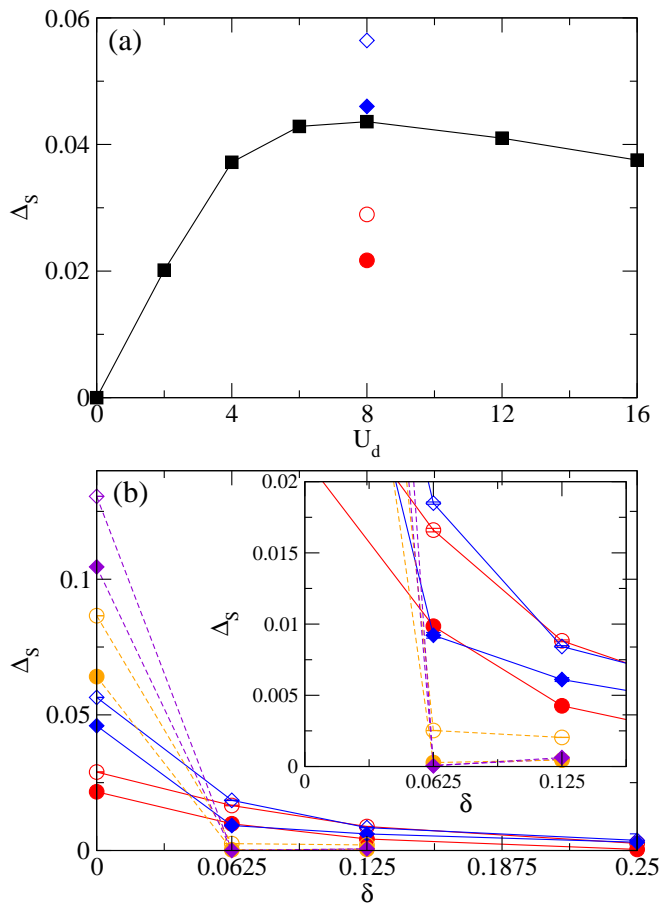


FIG. 3. (Color online) (a) Spin gap versus U_d in the undoped three-band ladder. Squares: $U_p = U_d/2, t_{pp} = 0.5$; Open circle: $U_p = 0, t_{pp} = 0$; Open diamond: $U_p = 0, t_{pp} = 0.5$; Filled circle: $U_p = 3, t_{pp} = 0$; Filled diamond: $U_p = 3, t_{pp} = 0.5$. In all cases $t_{dp}^\perp = 1$. (b) Same as a function of doping δ . Solid (dotted) lines correspond to $t_{dp}^\perp = 1$ ($|t_{dp}^\perp| = 1.25$). Open circles: $U_p = 0, t_{pp} = 0$; Open diamonds: $U_p = 0, t_{pp} = 0.5$; Filled circles: $U_p = 3, t_{pp} = 0$; Filled diamonds: $U_p = 3, t_{pp} = 0.5$; Lines are guides to the eye. The inset magnifies the small doping region. DMRG truncation and finite-size extrapolation errors are smaller than the symbol size.

III. COMPUTATIONAL RESULTS

In what follows, the computational results are for the geometry of Fig. 1(a), unless it is explicitly mentioned that they are for the geometry of Fig. 1(b).

A. Charge densities

In Table I we have given the calculated $L \rightarrow \infty$ extrapolated charges (see Supplemental Material [28] for the details of the extrapolation procedure) on the Cu-ions $\langle n_{Cu} \rangle$, rung O-ions $\langle n_{O_R} \rangle$ and leg O-ions $\langle n_{O_L} \rangle$, respectively, for $\delta = 0$ and $\delta = 0.125$, which are representative for other δ (see Supplemental Material [28]). The

TABLE I. Average extrapolated charge densities on Cu and O-sites in the undoped and doped ($\delta = 0.125$) three-band Hubbard Hamiltonian for $U_d = 8$.

U_p	t_{pp}	$\langle n_{Cu} \rangle$		$\langle n_{O_R} \rangle$		$\langle n_{O_L} \rangle$	
		$\delta=0$	$\delta=0.125$	$\delta=0$	$\delta=0.125$	$\delta=0$	$\delta=0.125$
0	0.0	0.81	0.82	0.13	0.19	0.12	0.20
0	0.5	0.73	0.75	0.22	0.28	0.15	0.22
3	0.0	0.82	0.84	0.12	0.18	0.12	0.19
3	0.5	0.75	0.78	0.20	0.26	0.14	0.21

doping-induced increase in $\langle n_{Cu} \rangle$ is very small, with the bulk of the doped charge going to O-ions. Importantly, given that there occur two leg O-ions corresponding to each rung O, the overall increase in population due to doping is larger for O_L than O_R . Our calculated charge densities are close to those obtained previously for shorter three-band ladders for similar parameters [24]. The calculated Cu-ion charge densities are very close to those in reference 24, where however, the calculations are for the geometry of Fig. 1(b). The nearly same Cu-ion charge densities for the two geometries is because the hole density on the outer O-ions are quite small [24]. This already suggests similar behavior of superconducting pair correlations in the two geometries, which we indeed find to be true.

B. Spin gaps, doped versus undoped

Fig. 3(a) shows the extrapolated spin gaps $\Delta_S = E(S_z = 1) - E(S_z = 0)$, where $E(\dots)$ is the lowest energy of the state with total z -component of spin S_z , for $\delta = 0$, $t_{dp}^\perp = 1$ and for a range of U_d for $U_p = U_d/2$ (see Supplemental Material [28] for details of the extrapolation procedure). For parameters for which previous calculations exist in the literature (for e.g., $U_d = 8, t_{dp}^\perp = 1, t_{pp} = U_p = 0$) our calculated Δ_S are the same as before [23]. The increase in Δ_S with t_{pp} for $\delta = 0$ has been noted before [24], and can be understood within perturbation theory [29]. Nonzero U_p suppresses Δ_S strongly. The behavior of Δ_S versus $U_d/|t_{pd}|$ is very similar to that versus $U/|t|$ in one-band ladders, where also a maximum near $U/|t| = 8$ is observed [14]. Undoped three- and one-band models are thus indeed similar.

In Fig. 3(b) we have shown the doping dependence of the extrapolated spin gaps (see Supplemental Material [28] for details of the extrapolations). We have included additional data points for $t_{dp}^\perp = 1.25$ here. Δ_S is suppressed strongly with doping, as is also true within the one-band ladder. Importantly, it appears that the larger is the spin gap in the undoped state, the more rapid is the suppression of the spin gap with doping. This is particularly obvious from comparison of $t_{dp}^\perp = 1.25$ versus 1.0. Equally interesting is the strong enhancement of Δ_S in the undoped state when $t_{pp} \neq 0$, as noted above, but

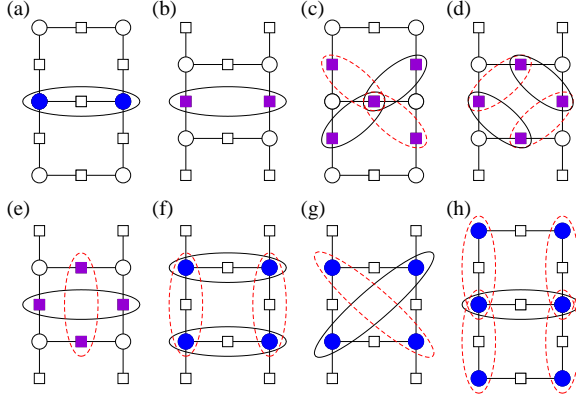


FIG. 4. (Color online) Pair symmetries we considered. Ellipses represent singlets (a) copper rung singlet, (b) oxygen leg singlet, (c) type 0, (d) type 1, (e) type 2, (f) type 3, (g) type 4, and (h) type 5. In (d)-(h) singlets represented by solid and dashed ellipses have opposite sign; for pair types (c)-(h) we considered both “s-wave” pairing, with all singlets having positive sign, and “d-wave” pairing, with the solid (dashed) singlets having sign $+1$ (-1).

very rapid suppression of the same upon doping. We further note that the detrimental effects of nonzero U_p and t_{pp} are synergistic, as seen from the inset of Fig. 3(b), where the spin gap at $\delta = 0.0625$ for $(U_p, t_{pp}) = (3.0, 0.0)$ and $(3.0, 0.5)$ are the same, even as for $\delta = 0$ the spin gap is larger by more than a factor of 2 for $(U_p, t_{pp}) = (3.0, 0.5)$. The very large Δ_S for $\delta = 0$, $t_{dp}^\perp = 1.25$, along with $\Delta_S \simeq 0$ for the doped cases here are in agreement with previous one-band calculation of the spin gap in the doped ladder [30] for $U = 8$ and $t_\perp/t > 1.5$.

The very rapid diminishing of Δ_S with doping already suggests the suppression of the superconducting correlations we find (see below).

C. Superconducting pair-pair correlations

1. Rung singlet pairs

For direct comparison of superconducting correlations with single-band ladders we have evaluated the pair-pair correlation function $P(r) = \langle P_i^\dagger P_j \rangle$, with $r = |i - j|$, where P_i^\dagger is the Cu-Cu ladder rung spin-singlet (see Fig. 4(a)), defined as $2^{-1/2}(d_{i,1,\uparrow}^\dagger d_{i,2,\downarrow}^\dagger - d_{i,1,\downarrow}^\dagger d_{i,2,\uparrow}^\dagger)$. Figs. 5(a) and (b) show the ladder length dependence of $P(r)$ for two different parameters sets, Fig. 5(a) with $U_p = t_{pp} = 0$ and Fig. 5(b) with $U_p = 3$ and $t_{pp} = 0.5$. For all of the ladder lengths and parameter values we studied, $P(r)$ was well fit by a power law $r^{-\alpha}$, provided short and long distances are excluded. These limits are due to finite size effects and are well understood in the case of the one-band ladder [18]. In particular, the sharp decrease in $P(r)$ for $r > L/2$ in Figs. 5 and 6 is a finite-size effect and not due to insufficiently large DMRG m .

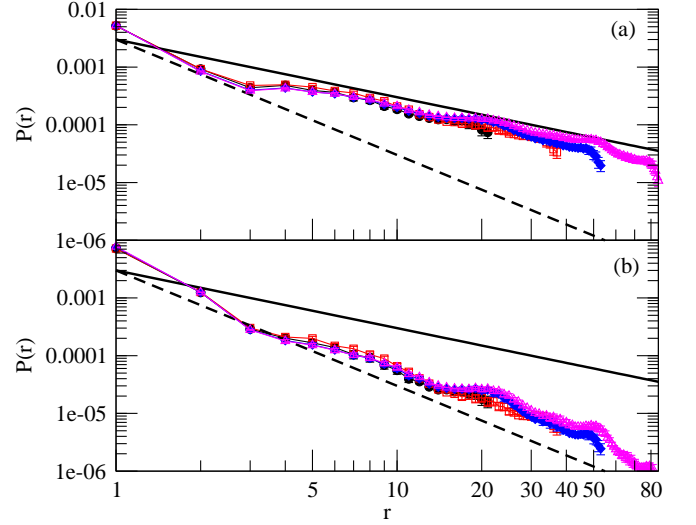


FIG. 5. (Color online) Pair-pair correlation function $P(r)$ with $U_d = 8$ and doping $\delta = 0.0625$ as a function of the rung distance r , for (a) $U_p = 0$ and $t_{pp} = 0$, and (b) $U_p = 3$ and $t_{pp} = 0.5$. Circles, squares, diamonds, and triangles are for 32, 48, 64, and 96 rung ladders, respectively. $P(r)$ data is extrapolated in the DMRG truncation error; error bars are calculated from lattice averaging (see text). The solid (dashed) lines are power laws r^{-1} (r^{-2}).

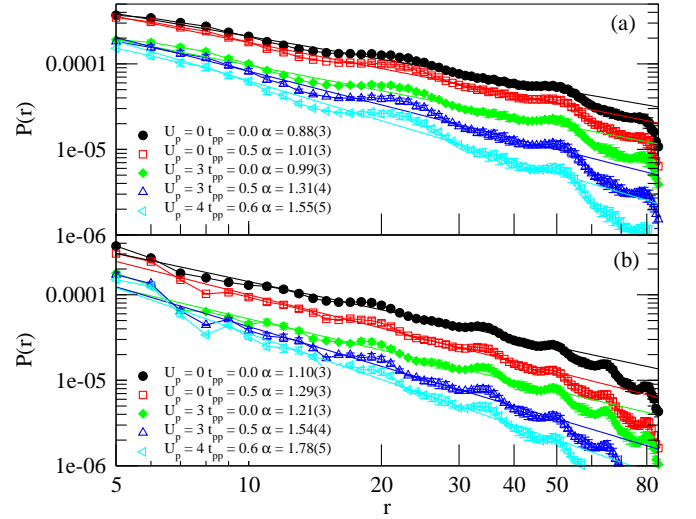


FIG. 6. (Color online) $P(r)$ as a function of the rung distance r for a 96-rung ladder with $U_d = 8$, for (a) doping $\delta = 0.0625$, and (b) $\delta = 0.1250$. Lines are linear fits of $P(r)$ for $10 \leq r \leq 48$; the power law exponents α are given in the figure legends.

As seen in Fig. 5(a), for $U_p = t_{pp} = 0$ we find $\alpha \sim 1$. With more realistic parameters, $U_p = 3$ and $t_{pp} = 0.5$, we find the power law exponent α close to 1.5 (see Fig. 5(b)).

In Fig. 6 we show power-law fits for $\delta = 0.0625$ (Fig. 6(a)) and $\delta = 0.125$ (Fig. 6(b)) for the 96-rung ladder. Nonzero U_p and t_{pp} both suppress $P(r)$, and

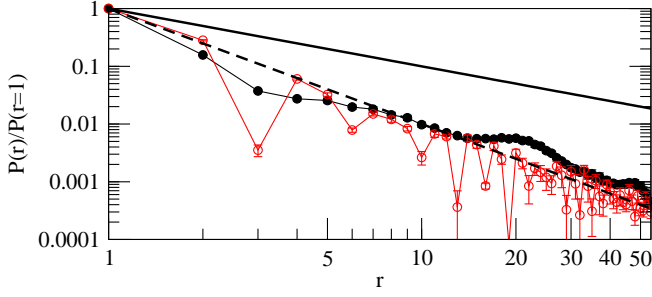


FIG. 7. (Color online) Rung-singlet $P(r)$ for the 64-rung lattice with $U_d = 8$, $U_p = 3$, $t_{pp}=0.5$, and $\delta = 0.0625$. $P(r)$ is normalized by its value at $r = 1$. Solid (open) symbols are for lattice of Fig. 1(a) (Fig. 1(b)). The solid (dashed) lines are power laws r^{-1} (r^{-2}).

when *both* are nonzero the suppression of $P(r)$ is further increased. This is consistent with the synergistic suppression of the spin gap in the doped ladder. As in the one-band ladder, we find that α increases rapidly with doping [18].

As mentioned above, we have also performed calculations of the rung singlet superconducting pair correlations for the ladder with the geometry of Fig. 1(b). The results of these calculations are shown in Fig. 7, where we compare the distance dependences of the normalized rung singlet pair-pair correlations for the two geometries of Fig. 1. The distance dependence of the pair correlations for the geometry of Fig. 1(b) with outer O ions included is as rapid as that for geometry of Fig. 1(a). As we point out below, this result is to be anticipated from physical reasonings.

2. Other pairing symmetries

Given that the doped holes primarily occupy the O_R and O_L sites investigation of pair-pair correlations beyond those involving simple rung singlets is important (note that the overall charges continue to reside primarily on the Cu-ions though). We investigated several different pair symmetries composed of superpositions of singlets on Cu and O atoms. The pair symmetries we investigated are shown in Fig. 4. We have calculated $P(r \equiv |i-j|) = \langle P_i^\dagger P_j \rangle$ for these different pairing symmetries for a 32-rung ladder with $U_d = 8$, $\Delta_{dp} = 3$, $U_p = 3$ and $t_{pp} = 0.5$, for doping $\delta = 0.125$. Our results are summarized in Figs. 8 and 9, where we compare the distance dependences of these pair correlations with the original pair correlation involving rung singlets only (Fig. 4(a)). As seen in Figs 8 and 9, all of the pairing symmetries we investigated fall into one of two categories:

1. $P(r)$ has identical long distance decay with $P(r)$ for the rung singlet correlation (Fig. 4(a)). This includes Fig. 4(b), Fig. 4(e) (s-wave only), Fig. 4(f) (s-wave only) and Fig. 4(h). These pair symmetries either contain within their superposition of pairs the rung singlet it-

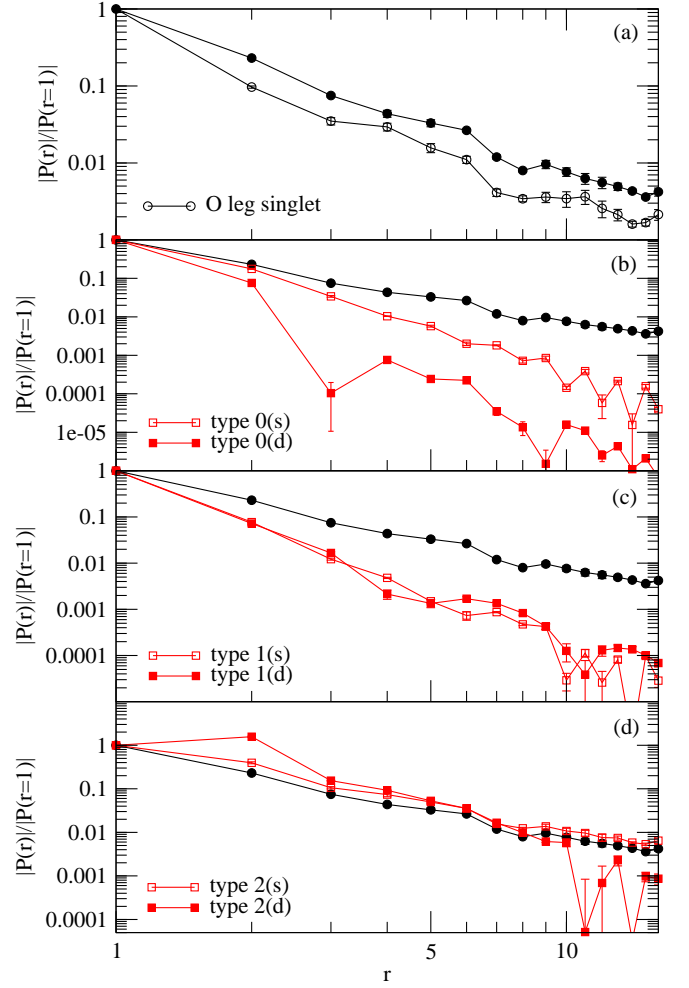


FIG. 8. (Color online) Pair-pair correlations for 32-rung ladders of Fig. 1(a) for the oxygen based pair symmetries in Fig. 4. Parameters are $U_d = 8$, $U_p = 3$, $t_{pp} = 0.5$, and $\delta = 0.125$. All $P(r)$ are normalized by their $r = 1$ value; we have taken absolute values of correlations that are negative. (a) pair symmetry of Fig. 4(b); (a) pair symmetry of Fig. 4(c); (c) pair symmetry of Fig. 4(d); (d) pair symmetry of Fig. 4(e); Round symbols are for Cu rung pairs (Fig. 4(a)), square open (filled) symbols are for *s* and *d*-wave pairing of the specified type (see text).

self, or in case of Fig. 4(b) a singlet between O atoms immediately adjacent to the Cu rung atoms.

2. $P(r)$ decays much faster with distance than the rung singlet correlation. This includes Figs. 4(c) and (d), Fig. 4(e) (d-wave only), Fig. 4(f) (d-wave only) and Fig. 4(g).

Based on these results we conclude that superconducting pair-pair correlations in the three-band ladder in general decay much faster than in the single-band ladder, and for realistic correlation and hopping parameters this decay precludes quasi-long range order.

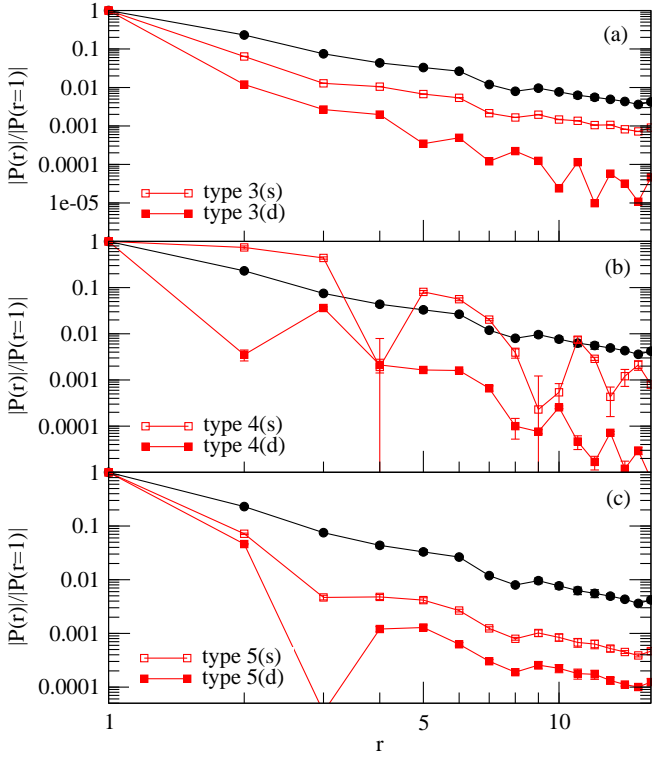


FIG. 9. (Color online) Pair-pair correlations for 32-rung ladders of Fig. 1(a) for the copper based pair symmetries in Fig. 4. Hamiltonian parameters are identical to Fig. 8. All $P(r)$ are normalized by their $r = 1$ value; we have taken absolute values of correlations that are negative. (a) pair symmetry of Fig. 4(f); (b) pair symmetry of Fig. 4(g); (c) pair symmetry of Fig. 4(h). Round symbols are for Cu rung pairs (Fig. 4(a)), square open (filled) symbols are for s and d -wave pairing of the specified type (see text).

D. Density oscillations

In the Luther-Emery phase, the long-distance decay of pair-pair correlations follows a power law determined by the correlation parameter κ_ρ , with $P(r) \propto r^{-1/\kappa_\rho}$ ($\alpha = 1/\kappa_\rho$). Similarly, density-density correlations $N(r)$ follow a power law with $N(r) \propto r^{-\kappa_\rho}$ ($N(r = |i - j|) = \langle n_i n_j \rangle - \langle n_i \rangle \langle n_j \rangle$, where n_i is the charge density operator for site i). Pairing correlations decay slower than $1/r$ and dominate over density-density correlations only for $\kappa_\rho > 1$. Density correlations provide a second estimate of κ_ρ and consistency check.

In the 2-leg one-band ladder, charge density (Friedel) oscillations can be fit to accurately extract κ_ρ [18, 31]. We use a similar procedure in our three-band model calculations. We fit the charge density to the following function [18, 31]

$$n_j = A \frac{\cos(\pi N_h j / L_{\text{eff}} + \phi)}{\sin(\pi j / L)^{\kappa_\rho/2}} + n_0. \quad (2)$$

In Eq. 2, n_j is the charge density in the j th unit cell of the lattice; n_j is the sum of the charge densities of the

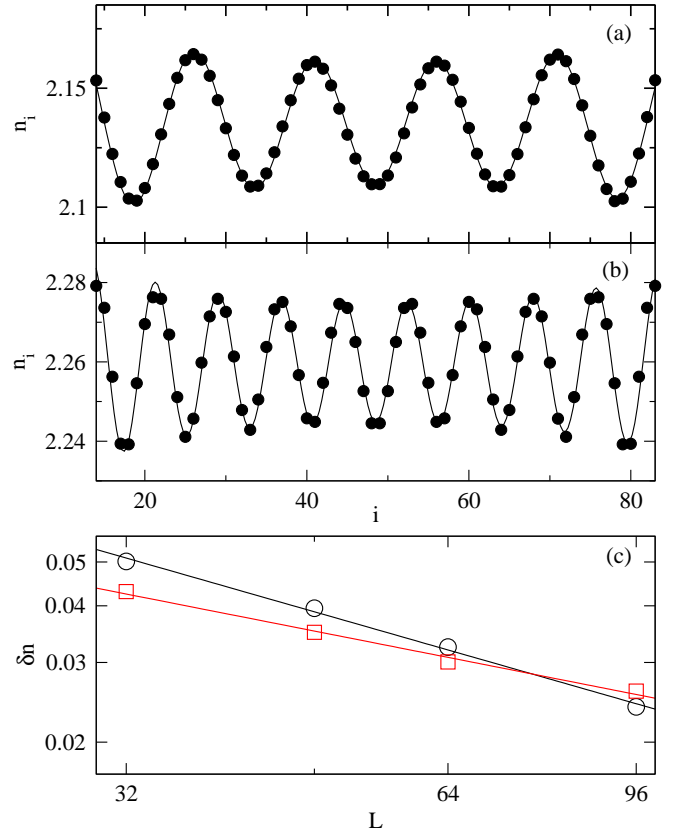


FIG. 10. (Color online) (a) Total charge density versus rung index i for a 96-rung ladder with $U_p = 4$, $t_{pp} = 0.6$, and $\delta = 0.0625$. The line is a fit to Eq. 2. (b) Same as (a) but $\delta = 0.125$. (c) Amplitude of density oscillations at $L/2$ versus ladder length. Circles (squares) are for $U_p = 0$ ($U_p = 4$), $t_{pp} = 0$ ($t_{pp} = 0.6$), and $\delta = 0.0625$. Lines are fits (see text).

rung copper and oxygen atoms, plus the charge densities on two adjacent leg oxygen atoms. N_h is the number of holes, A the overall amplitude, ϕ a phase shift, and n_0 the background charge density. L_{eff} is an effective length that is less than L because of the finite extent of holes [18]. We performed a nonlinear fit of the charge density to Eq. 2 in the central region of the ladders for $L=32, 48, 64$, and 96 , keeping A , n_0 , κ_ρ , and ϕ as free parameters. Fig. 10(a) and (b) show representative fits for $L = 96$. While in the one-band ladder a good fit was found [18] with $L_{\text{eff}} = L - 2$, we found a shorter L_{eff} in the three-band ladder, for example $L_{\text{eff}} \approx L - 9$ and $L - 6$ for $\delta = 0.0625$ and $\delta = 0.125$, respectively. This shows that doped holes extend over a larger number of lattice sites in the three-band ladder than in the one-band ladder (see also Section III E).

The value of κ_ρ can be most accurately determined in ladders [18] from the scaling of the amplitude of the density oscillations in the center of the ladder,

$$\delta n(L) = n(L/2) - n_0 \propto L^{-\kappa_\rho/2}. \quad (3)$$

In Eq. 3 we determined $n(L/2)$ and n_0 from the fit of

δ	U_p	t_{pp}	κ_ρ	
			$P(r) (L=96)$	$\delta n (L \rightarrow \infty)$
0.0625	0.0	0.0	1.14(4)	1.35(6)
	0.0	0.5	0.99(3)	1.22(2)
	3.0	0.0	1.01(3)	1.20(6)
	3.0	0.5	0.76(2)	0.97(1)
	4.0	0.6	0.65(2)	0.93(5)
0.125	0.0	0.0	0.91(2)	1.08(6)
	0.0	0.5	0.78(2)	0.93(2)
	3.0	0.0	0.83(2)	1.08(3)
	3.0	0.5	0.65(2)	0.80(4)
	4.0	0.6	0.56(2)	0.75(8)

TABLE II. Correlation exponents κ_ρ obtained from fitting $P(r)$ (Section III C) and density oscillations (Section III D).

Eq. 2. Fig. 10(c) shows typical results for δn for two different parameter sets (see [28] for other parameter values). We then estimated κ_ρ in the $L \rightarrow \infty$ limit from a linear fit as was done for the one-band ladder [18]. Table II summarizes our results for κ_ρ as determined from directly fitting $P(r)$ and from Eq. 3. In comparison, the value of κ_ρ in the single band ladder is 1.54–1.66 at $\delta = 0.0625$ and 0.92–1.17 at $\delta = 0.125$ [18], roughly consistent with our $U_p = t_{pp} = 0$ values. In general, the $L \rightarrow \infty$ κ_ρ determined from density oscillations is larger than the value found from the $L = 96$ pair-pair correlations, with a larger finite-size correction at $\delta = 0.0625$ than at $\delta = 0.125$. A slight decrease in the power-law slope of $P(r)$ with increasing size is evident in Fig. 5, so we believe that the results from fitting $P(r)$ and δn are consistent with each other.

We note that the κ_ρ calculated from the two different methods display *nearly identical* dependence on U_p and t_{pp} . The effects of nonzero U_p and t_{pp} are not simply additive. Rather (see Table II), the decrease of κ_ρ is larger when *both* U_p and t_{pp} are nonzero compared to the sum of the changes in κ_ρ with ($U_p > 0, t_{pp} = 0$) or ($U_p = 0, t_{pp} > 0$). We note that we cannot rule out the possibility that $\kappa_\rho > 1$ in the limit of very small doping; indeed we find $\kappa_\rho \sim 1$ for $\delta = 0.0625$ even with realistic U_p and t_{pp} . However, if one takes the doping typically assumed as maximizing pairing in the 2D one-band Hubbard model ($\delta = 0.125$), we find that κ_ρ is significantly less than one, even considering our computational and finite-size errors. This indicates the absence of the quasi-long range SC characteristic of the single-band ladder.

E. Suppression of pair correlations, a physical picture

The suppression of the pair-pair correlations within the multi-band model is reminiscent of similar suppression of the same correlations for large rung hopping $t_\perp > t$

within the one-band model (see Fig. 6 in reference 15). As seen in reference 15 not only is the one-band pair-pair correlation suppressed by large t_\perp , the suppression occurs at smaller and smaller t_\perp (that are however > 1) as the Hubbard repulsion U increases. Within the same range of U the spin gap in the undoped one-band ladder *increases* with U . It therefore follows that *increase in the spin gap in the undoped one-band ladder is accompanied by concomitant increase of pair correlations in the doped ladder, only until a maximum in the undoped ladder spin gap is reached*. Beyond this maximum, further increase of the spin gap in the undoped single-band ladder results in suppression of the pair-pair correlations in the doped ladder. *Our results in Figs. 6-9 indicate that this maximum in the spin gap of the undoped three-band ladder has been reached already at $t_{dp}^\perp = 1$.* We argue in the following that this is due to the large pair-breaking effect in the multi-band ladder.

Superconducting pairing involving rung singlets in both one- and multi-band ladder Hamiltonians can understood within an *effective* Hamiltonian of the form,

$$H_{\text{eff}} = \sum_i J(\delta) P_i^\dagger P_i - t_{\text{pair}} \sum_{\langle i,j \rangle} P_i^\dagger P_j - t_f \sum_{\langle \mu,\nu \rangle, \sigma} f_{\mu,\sigma}^\dagger f_{\nu,\sigma} \quad (4)$$

where $J(\delta)$ is proportional to the self-consistent spin gap at doping δ , t_{pair} the effective pair hopping integral, and t_f refers to single-particle fermion hops. Here i and j refer to rung indices. While μ, ν refer to Cu-ions on nearest neighbor rungs in the one-band ladder, they refer to both Cu- and O-sites in the multi-band ladder. Within the one-band model, t_{pair} and t_f are related, with $t_{\text{pair}} \sim t_f^2 / \Delta_{\text{pb}}$, where Δ_{pb} is the pair-binding energy, roughly proportional to the spin gap in the doped ladder.

The interactions $J(\delta)$ and t_{pair} , taken together, dominate over the pair-breaking single-particle t_f over a broad range of parameters in the one-band ladder, including in particular $t_\perp = 1$. This situation is altered significantly within the multi-band model. The doped holes now enter primarily O-sites (see Table 1), and the complete spin-singlet wavefunction involves not only the Cu-ions but also the rung O-ion and the four ladder oxygens on either side of the rung. Pair motion now must involve not only the doped charges on the Cu-ions of a rung, but also those on the neighboring O-ions, making the effective mass of the spin-singlet within the three-band model considerably larger than in the one-band model. At the same time, however, t_f now can involve the holes on the O-ions exclusively, with the Cu-ion holes playing a very limited role (*i.e.*, t_f now includes and is even dominated by t_{pp}). Consequently, the effective t_{pair} is smaller and the effective t_f larger within the three-band model. *Single-particle hopping thus has a far stronger pair-breaking effect in the three-band ladder.*

Based on the above it now becomes obvious why the strongest suppression of the doped-state spin gap and rung singlet superconducting pair correlations occur within the Hamiltonians with nonzero t_{pp} (see Figs. 3(b)

and 6). With the geometry of Fig. 1(b), the effective mass of the spin-singlet is further enhanced while the additional t_{pp} contribute to additional t_f and pair-breaking. The strong suppression of pair correlations should therefore be common to the geometries of Fig. 1(a) and (b), as indeed is found numerically.

IV. DISCUSSIONS AND CONCLUSION

Our theoretical results demonstrate that, (i) conclusions regarding pairing based on effective single-band ladder models cannot be extended to the three-band ladder, and (ii) there is no pairing within the three-band ladder for realistic cuprate parameters $U_p = 3-4$, $t_{pp} = 0.5-0.6$ [25]. U_p and t_{pp} both suppresses pairing uniformly.

The absence of SC in the 2-leg ladder compound $\text{La}_{2-x}\text{Sr}_x\text{CuO}_{2.5}$ [32] is therefore expected within our theory. Superconducting $\text{Sr}_{14-x}\text{Ca}_x\text{Cu}_{24}\text{O}_{41}$ consists of alternating planes of corner-sharing CuO_2 chains and edge-sharing Cu_2O_3 ladders [33–35]. It is believed that there occur nearly 5 holes per formula unit (f. u.) on chains and 1 hole per f. u. on ladders at $x = 0$. There occurs some transfer of holes from chain to ladder with increasing x , but the actual extent of the transfer is not agreed upon [36]. The appearance of SC above 4.0 GPa in $x = 11.5$ single crystals is accompanied by a 1D-to-2D dimensional crossover, as evidenced from the insulator-like resistivity ρ_a along the rung-axis a at all temperatures below the critical pressure and metallic ρ_a at all temperatures above this pressure [34]. The resistivity ratio ρ_a/ρ_c (the c -axis corresponds to the ladder leg direction) of the $x = 11.5$ compound decreases by more than a factor of 4 at low temperature and high pressure [34]. There occurs a concomitant decrease in the a -axis lattice parameter, although at still higher pressure where superconducting T_c decreases the lattice parameter increases again. ^{63}Cu and ^{17}O NMR studies for the $x = 12$ compound have found that the spin gap decreases sharply with pressure, and there appear low-lying spin excitations, indicating the presence of mobile quasi-particles that contribute to a finite density of states at the Fermi level and perhaps also SC [37, 38]. Taken together, these observations, (i) indicate clearly that the origin of SC in $\text{Sr}_{14-x}\text{Ca}_x\text{Cu}_{24}\text{O}_{41}$ cannot be found within ladder-based theories [35], and

(ii) are consistent with our finding that superconducting correlations are absent in the three-band ladder Hamiltonian with realistic U_p and t_{pp} .

Our results raise a fundamental (and disturbing) question. What is the implication of the absence of a Luther-Emery superconducting phase [13] in the three-band 2-leg ladder Hubbard Hamiltonian for the 2D CuO_2 layer? We make the following observations. First, theories of cuprate SC that assume a gapped spin-liquid phase proximate to the superconducting state [1, 3, 17, 20, 39] cannot be justified by the demonstration of quasi-long range superconducting correlations within the one-band ladder-based theories. The one-band ladder model is an artificial one with no relationship to real cuprates. Second, the profound difference between the results of one- and three-band ladder calculations (understandable physically with hindsight, see Section III.D) suggests that the mapping of the three-band Hamiltonian to the one-band Hubbard model [5] is correct only for a limited choice of parameters. In the context of cuprates, the applicability of the mapping across doping levels, realistic geometries and parameters (especially t_{pp}) has been questioned by other authors [40–42], although these criticisms themselves remain controversial. Our work suggests that re-evaluation of these earlier works is necessary. Finally, as with the 2D one-band Hubbard Hamiltonian, numerical computation of $d_{x^2-y^2}$ pair correlations within the three-band Hamiltonian for the CuO_2 layer also found absence of SC [43]. This latter work used the constrained path quantum Monte Carlo approach that relies on a trial wavefunction to eliminate the Fermion sign problem. The calculations were also based on relatively small lattices. Our DMRG calculations, devoid of sign errors, provide strong support to the conclusions of reference 43. Taken together, these observations suggest that a comprehensive theory of cuprate SC may require starting hypotheses or models that are significantly different from existing ones.

Work at Arizona was supported by NSF-CHE-1764152. Some calculations in this work were supported under project TG-DMR190068 of the Extreme Science and Engineering Discovery Environment [44] (XSEDE), which is supported by National Science Foundation grant number ACI-1548562. Specifically, we used the Bridges and Bridges2 systems at the Pittsburgh Supercomputing Center, which are supported by NSF awards ACI-1445606 and ACI-1928147, respectively.

[1] P. W. Anderson, G. Baskaran, Z. Zou, and T. Hsu, Resonating valence-bond theory of phase transitions and superconductivity in La_2CuO_4 -based compounds, *Phys. Rev. Lett.* **58**, 2790 (1987).
[2] P. W. Anderson, P. A. Lee, M. Randeria, T. M. Rice, N. Trivedi, and F. C. Zhang, The physics behind high-temperature superconducting cuprates: the ‘plain vanilla’ version of RVB, *J. Phys. Condens. Matter* **16**, R755 (2004).

[3] P. A. Lee, N. Nagaosa, and X. G. Wen, Doping a Mott insulator: Physics of high-temperature superconductivity, *Rev. Mod. Phys.* **78**, 17 (2006).
[4] D. J. Scalapino, A common thread: The pairing interaction for unconventional superconductors, *Rev. Mod. Phys.* **84**, 1383 (2012).
[5] F. C. Zhang and T. M. Rice, Effective Hamiltonian for the superconducting Cu oxides, *Phys. Rev. B* **37**, 3759(R) (1988).

- [6] S. Zhang, J. Carlson, and J. E. Gubernatis, Pairing correlations in the two-dimensional Hubbard model, *Phys. Rev. Lett.* **78**, 4486 (1997).
- [7] T. Aimi and M. Imada, Does simple two-dimensional Hubbard model account for high- T_c superconductivity in copper oxides?, *J. Phys. Soc. Jpn.* **76**, 113708 (2007).
- [8] M. Qin, C.-M. Chung, H. Shi, E. Vitali, C. Hubig, U. Schollwöck, S. R. White, and S. Zhang, Absence of superconductivity in the pure two-dimensional Hubbard model, *Phys. Rev. X* **10**, 031016 (2020).
- [9] Z. B. Huang, H. Q. Lin, and J. E. Gubernatis, Quantum Monte Carlo study of spin, charge, and pairing correlations in the t - t' - U Hubbard model, *Phys. Rev. B* **64**, 205101 (2001).
- [10] C.-M. Chung, M. Qin, S. Zhang, U. Schollwöck, and S. R. White, Plaquette versus ordinary d -wave pairing in the t' -Hubbard model on a width 4 cylinder, *Phys. Rev. B* **102**, 041106(R) (2020).
- [11] N. Gomes, W. W. De Silva, T. Dutta, R. T. Clay, and S. Mazumdar, Coulomb enhanced superconducting pair correlations in the frustrated quarter-filled band, *Phys. Rev. B* **93**, 165110 (2016).
- [12] J. Venderley and E.-A. Kim, Density matrix renormalization group study of superconductivity in the triangular lattice hubbard model, *Phys. Rev. B* **100**, 060506(R) (2019).
- [13] A. Luther and V. J. Emery, Backward scattering in the one-dimensional electron gas, *Phys. Rev. Lett.* **33**, 589 (1974).
- [14] R. M. Noack, S. R. White, and D. J. Scalapino, Correlations in a two-chain Hubbard model, *Phys. Rev. Lett.* **73**, 882 (1994).
- [15] R. M. Noack, N. Bulut, D. J. Scalapino, and M. G. Zacher, Enhanced $d_{x^2-y^2}$ pairing correlations in the two-leg Hubbard ladder, *Phys. Rev. B* **56**, 7162 (1997).
- [16] L. Balents and M. P. A. Fisher, Weak-coupling phase diagram of the two-chain Hubbard model, *Phys. Rev. B* **53**, 12133 (1996).
- [17] K. Le Hur and T. M. Rice, Superconductivity close to the Mott state: From condensed-matter systems to the superfluidity in optical lattices, *Ann. Phys.* **324**, 1452 (2009).
- [18] M. Dolfi, B. Bauer, S. Keller, and M. Troyer, Pair correlations in doped Hubbard ladders, *Phys. Rev. B* **92**, 195139 (2015).
- [19] Y. Gannot, Y.-F. Jiang, and S. A. Kivelson, Hubbard ladders at small U revisited, *Phys. Rev. B* **102**, 115136 (2020).
- [20] V. J. Emery, S. A. Kivelson, and O. Zachar, Spin-gap proximity effect mechanism of high-temperature superconductivity, *Phys. Rev. B* **56**, 6120 (1997).
- [21] A. E. Feiguin, S. R. White, D. J. Scalapino, and I. Affleck, Pairing symmetry and Josephson current in doped 2-leg t - J ladders, *Phys. Rev. Lett.* **101**, 217001 (2008).
- [22] E. Dagotto and T. M. Rice, Surprises on the way from one- to two-dimensional quantum magnets: the ladder materials, *Science* **271**, 618 (1996).
- [23] E. Jeckelmann, D. J. Scalapino, and S. R. White, Comparison of different ladder models, *Phys. Rev. B* **58**, 9492 (1998).
- [24] S. Nishimoto, E. Jeckelmann, and D. J. Scalapino, Differences between hole and electron doping of a two-leg CuO ladder, *Phys. Rev. B* **66**, 245109 (2002).
- [25] M. Hirayama, Y. Yamaji, T. Misawa, and M. Imada, Ab initio effective Hamiltonians for cuprate superconductors, *Phys. Rev. B* **98**, 134501 (2018).
- [26] M. Fishman, S. R. White, and E. M. Stoudenmire, The ITensor software library for tensor network calculations (2020), <https://arxiv.org/abs/2007.14822>.
- [27] E. M. Stoudenmire and S. R. White, Real-space parallel density matrix renormalization group, *Phys. Rev. B* **87**, 155137 (2013).
- [28] See Supplemental Material at <http://link.aps.org/supplemental/xx.xxxx> for further details of calculations.
- [29] H. Eskes and J. H. Jefferson, Superexchange in the cuprates, *Phys. Rev. B* **48**, 9788 (1993).
- [30] R. M. Noack, S. R. White, and D. J. Scalapino, The ground state of the two-leg Hubbard ladder A density-matrix renormalization group study, *Physica C* **270**, 281 (1996).
- [31] S. R. White, I. Affleck, and D. J. Scalapino, Friedel oscillations and charge density waves in chains and ladders, *Phys. Rev. B* **65**, 165122 (2002).
- [32] Z. Hiroi and M. Takano, Absence of superconductivity in the doped antiferromagnetic spin-ladder compound $(\text{La,Sr})\text{CuO}_{2.5}$, *Nature* **377**, 41 (1995).
- [33] M. Uehara, T. Nagata, J. Akimitsu, H. Takahashi, N. Mori, and K. Kinoshita, Superconductivity in the ladder material $\text{Sr}_{0.4}\text{Ca}_{13.6}\text{Cu}_{24}\text{O}_{41.84}$, *J. Phys. Soc. Jpn.* **65**, 2764 (1996).
- [34] T. Nagata, M. Uehara, J. Goto, J. Akimitsu, N. Motoyama, H. Eisaki, S. Uchida, H. Takahashi, T. Nakanishi, and N. Mori, Pressure-induced dimensional crossover and superconductivity in the hole-doped two-leg ladder compound $\text{Sr}_{14-x}\text{Ca}_x\text{Cu}_{24}\text{O}_{41}$, *Phys. Rev. Lett.* **81**, 1090 (1998).
- [35] T. Vuletić, B. Korin-Hamzić, T. Ivek, S. Tomić, B. G. M. Dressel, and J. Akimitsu, The spin-ladder and spin-chain system $(\text{La,Y,Sr,Ca})_{14}\text{Cu}_{24}\text{O}_{41}$: Electronic phases, charge and spin dynamics, *Phys. Rep.* **428**, 169 (2006).
- [36] M. Bugnet, S. Loeffler, D. Hawthorn, H. A. Dabkowska, G. M. Luke, P. Schattschneider, G. A. Sawatzky, G. Radtke, and G. A. Botton, Real-space localization and quantification of hole distribution in chain-ladder $\text{Sr}_3\text{Ca}_{11}\text{Cu}_{24}\text{O}_{41}$ superconductor, *Sci. Adv.* **2**, e1501652 (2016).
- [37] Y. Piskunov, D. Jérôme, P. Auban-Senzier, P. Wzietek, and A. Yakubovsky, Spin excitations in the $(\text{Sr,Ca})_{14}\text{Cu}_{24}\text{O}_{41}$ family of spin ladders: ^{63}Cu and ^{17}O NMR studies under pressure, *Phys. Rev. B* **69**, 014510 (2004).
- [38] N. Fujiwara, Y. Fujimaki, S. Uchida, K. Matsubayashi, T. Matsumoto, and Y. Uwatoko, NMR and NQR study of pressure-induced superconductivity and the origin of critical-temperature enhancement in the spin-ladder cuprate $\text{Sr}_2\text{Ca}_{12}\text{Cu}_{24}\text{O}_{41}$, *Phys. Rev. B* **80**, 100503(R) (2009).
- [39] E. Arrigoni, E. Fradkin, and S. A. Kivelson, Mechanism of high-temperature superconductivity in a striped Hubbard model, *Phys. Rev. B* **69**, 214519 (2004).
- [40] D. C. Peets, D. G. Hawthorn, K. M. Shen, Y.-J. Kim, D. S. Ellis, H. Zhang, S. Komiyama, Y. Ando, G. A. Sawatzky, R. Liang, D. A. Bonn, and W. N. Hardy, X-ray absorption spectra reveal the inapplicability of the single-band Hubbard model to overdoped cuprate superconductors, *Phys. Rev. Lett.* **103**, 087402 (2009).
- [41] D. K. Sunko, Destabilization of the Zhang-Rice singlet

- at optimal doping, J. Exp. and Theor. Phys. **109**, 652 (2009).
- [42] C. P. J. Adolphs, S. Moser, G. A. Sawatzky, and M. Berciu, Non-Zhang-Rice singlet character of the first ionization state of T-CuO, Phys. Rev. Lett. **116**, 087002 (2016).
- [43] M. Guerrero, J. E. Gubernatis, and S. Zhang, Quantum Monte Carlo study of hole binding and pairing correlations in the three-band Hubbard model, Phys. Rev. B **57**, 11980 (1998).
- [44] J. Towns, T. Cockerill, M. Dahan, I. Foster, K. Gaither, A. Grimshaw, V. Hazlewood, S. Lathrop, D. Lifka, G. D. Peterson, R. Roskies, J. R. Scott, and N. Wilkins-Diehr, XSEDE: Accelerating scientific discovery, Computing in Science & Engineering **16**, 62 (2014).